2022

Critical new insights into the binding of poly- and perfluoroalkyl substances (PFAS) to albumin protein

Jessica L. Alesio

Angela L. Slitt
University of Rhode Island, aslitt@uri.edu

Geoffrey D. Bothun
University of Rhode Island, gbothun@uri.edu

Citation/Publisher Attribution

Alesio, J. L., Slitt, A., & Bothun, G. D. (2022). Critical new insights into the binding of poly- and perfluoroalkyl substances (PFAS) to albumin protein. *Chemosphere, 287*(1), 131979. https://doi.org/10.1016/j.chemosphere.2021.131979
Available at: https://doi.org/10.1016/j.chemosphere.2021.131979

Critical new insights into the binding of poly- and perfluoroalkyl substances (PFAS) to albumin protein

Critical new insights into the binding of poly- and perfluoroalkyl substances (PFAS) to albumin protein

Jessica L. Alesio,[a] Angela Slitt,[b] and Geoffrey D. Bothun*,[a]

[a]Department of Chemical Engineering, University of Rhode Island, 2 East Alumni Ave, Kingston, Rhode Island 02881, United States.

[b]Department of Biomedical and Pharmaceutical Sciences, University of Rhode Island, 7 Greenhouse Rd, Kingston, Rhode Island 02881, United States.

*Corresponding Author: Geoffrey D. Bothun. E-mail: gbothun@uri.edu, Tel: +1-401-874-9518

ABSTRACT

With an increasing number of health-related impacts of per- and polyfluoroalkyl substances (PFAS) being reported, there is a pressing need to understand PFAS transport within both the human body and the environment. As proteins can serve as a primary transport mechanism for PFAS, understanding PFAS binding to proteins is essential for predictive physiological models where accurate values of protein binding constants are vital. In this work we present a critical analysis of three common models for analyzing PFAS binding to bovine serum albumin (BSA) based on fluorescence quenching: the Stern-Volmer model, the modified Stern-Volmer model, and the Hill equation. The PFAS examined include perfluorooctanoic acid (PFOA), perfluorononanoic acid (PFNA), perfluorodecanoic acid (PFDA), perfluorobutanesulfonic acid (PFBS), perfluorohexanesulfonic acid (PFHxS), perfluorooctanesulfonic acid (PFOS), and the replacement compound 2,3,3,3-tetrafluoro-2-(heptafluoropropoxy)propanoate (HFPO-DA or GenX). While all three models capture the general effects of hydrophobicity and steric limitations to PFAS binding, the Hill equation highlighted a unique relationship between binding cooperativity and the number of fluorinated carbons, with PFOA exhibiting the greatest binding cooperativity. The significance of steric limitations was confirmed by comparing results obtained by fluorescence quenching, which is an indirect method based on specific binding, to those obtained by equilibrium dialysis where PFAS binding directly correlated with traditional measures of hydrophobicity. Finally, the binding constants were correlated with PFAS physicochemical properties where van der Waals volume best described the steric limitations observed by fluorescence quenching.

Keywords: PFAS, protein binding, albumin, equilibrium dialysis, fluorescence quenching

INTRODUCTION

Per- and polyfluoroalkyl substances (PFAS) are synthetic compounds produced for a wide range of applications including nonstick industrial and commercial products, textiles, and firefighting foams. Due to their persistence in the environment, human and ecosystem-related exposures can occur long after release (Domingo and Nadal, 2017). Ninety-eight percent of the United States population is expected to have detectable amounts of PFAS in their blood (Hu et al., 2016). Water treatment plants are not equipped to remove all PFAS from water and thus, drinking water creates another continuous exposure route (Ross et al., 2018). Although more robust remediation systems are being created for the legacy compounds such as perfluorooctanoic acid (PFOA) and perfluorooctanesulfonic acid (PFOS), shorter and longer PFAS may not respond to the new treatment systems (Ahrens and Bundschuh, 2014; Xiao et al., 2020). It is estimated that there are over 4,700 different PFAS and limited knowledge about even the simplest of compounds (Boston et al., 2019). Once these PFAS enter the body, they are linked to negative health effects such as immunosuppression, obesity, and insulin resistance (Cardenas et al., 2017; Grandjean and Budtz-Jørgensen, 2013; Hartman et al., 2017)

As the scientific community discovers more PFAS, there is a need to understand the effect on ecosystems and humans. Using bioaccumulation modeling, Ng and Hungerbühler (2014) explained that both protein and lipid association are vital to the adaptation of models for different PFAS. Dassuncao et al (2018) also used bioaccumulation modeling but were limited by information available related to protein binding and lipid association. Another predictive tool used is physiologically based pharmacokinetic/ pharmacodynamic (PBPK/PBPD) modeling but also requires accurate tissue-protein partitioning coefficients.

Due to the lack of PFAS protein binding data, researchers have used both computational models and laboratory experiments to obtain binding constants for different PFAS (Chen et al., 2015; Chen and Guo, 2009; Cheng and Ng, 2018; Fedorenko et al., 2021; Qin et al., 2010; Salvalaglio et al., 2010; Wu et al., 2009). Most of this work has been limited to legacy PFAS (PFOA and PFOS). Bovine serum albumin protein (BSA) and/or the human equivalent (HSA) are used because they are the most abundant in the blood and albumin has been shown to be the major carrier of PFAS in the body (Forsthuber et al., 2020). In addition to transport, serum protein binding of PFAS may provide insight into the effect of PFAS on the liver, as serum albumin is catabolized in the liver and kidneys (Gitlin et al., 1958). A limited number of studies have used equilibrium dialysis as a direct measure of the amount of PFAS bound to serum albumin (Allendorf et al., 2019; Bischel et al., 2010; Gao et al., 2019; Wu et al., 2009). This approach captures nonspecific interactions and specific binding events within the hydrophobic pocket of serum albumin.

A common but indirect method to determine PFAS binding to serum albumin has been fluorescence quenching (Chen et al., 2015; Chen and Guo, 2009; Hebert and MacManus-Spencer, 2010; Macmanus-spencer et al., 2010; Qin et al., 2010; Wu et al., 2009). Fluorescence quenching is a widely used spectroscopic technique that measures the binding of small organic molecules and ions to proteins based on the intrinsic fluorescence of amino acid residues within the protein structure. In bovine serum albumin (BSA, Figure S1), the fluorescence stems from two tryptophan (Trp) residues, one located within the hydrophobic cavity of the protein (Trp-213) and one closer the surface (Trp-134) and more accessible by the solvent (water) (Steinhardt et al., 1971). The quenching behavior of these Trp residues indicates the extent of proximal molecular binding and changes in the local polarity of the solvent environment, revealing

information about the binding mechanism. Limitations to the fluorescence quenching method include the assumptions behind the quenching models and the apparent lack of consensus as to the appropriate ratio of PFAS to albumin.

In our previous work, Fedorenko et al. (2021) examined the entropic driving force for PFAS binding to BSA using fluorine nuclear magnetic resonance spectroscopy (^{19}F-NMR) and concluded that binding occurs via both specific binding within the hydrophobic pocket as well as adsorption to the surface of the protein. Here, our aim was to examine how those different types of binding events influence the fluorescence quenching of BSA and to evaluate the three common models used to calculate PFAS-BSA association constants against equilibrium dialysis.

This work examined a range of perfluoroalkylcarboxylates (PFCA, $C_{7,F}$ to $C_{9,F}$ where $C_{x,F}$ denotes the number of fluorinated carbons), perfluoroalkylsulfonates (PFSA; $C_{4,F}$, $C_{6,F}$ and $C_{8,F}$), and the replacement compound 2,3,3,3-tetrafluoro-2-(heptafluoropropoxy)propanoate (GenX; $C_{5,F}$; note that only three carbons are perfluorinated) and established binding relationships for PFAS physicochemical properties (Scheme 1). Three different data analysis techniques were used to correlate fluorescence quenching with protein binding: the Stern-Volmer model, the modified Stern-Volmer model, and the Hill equation. Comparisons between fluorescence quenching and equilibrium dialysis results provided key insights into the underlying mechanisms. Relationships were established between octanol-water partitioning coefficients (log K_{ow}) as well as van der Waals volume and the extent of BSA binding to aid in prediction tools for the wide range of PFAS.

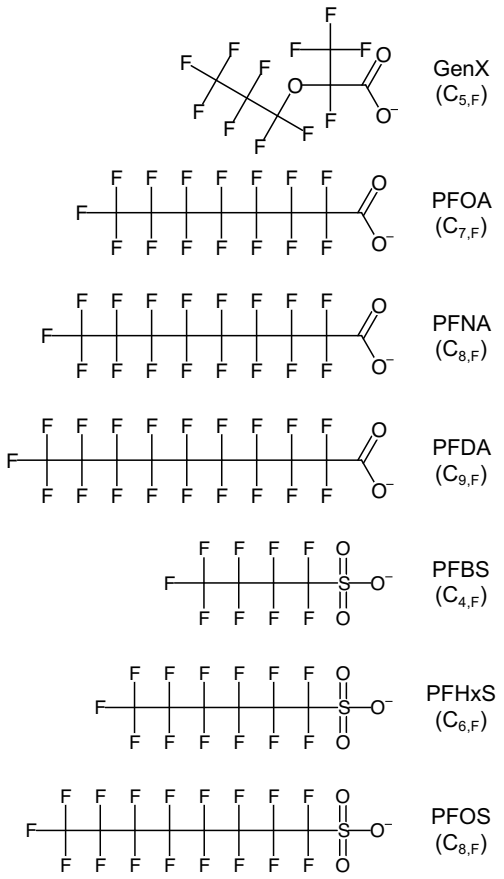

Scheme 1. PFAS examined. $C_{x,F}$ denotes the number of fluorinated carbons.

MATERIALS AND METHODS

Materials. Bovine serum albumin (lyophilized powder, 99% fatty acid free) was obtained from Sigma-Aldrich (St. Louis, MO). A BSA concentration of 1.25 μM in pH 7.4 phosphate buffered saline (1X PBS) was used in each fluorescence quenching experiment. The solution of BSA was kept at 4°C prior to use.

Perfluorooctanoic acid, perfluorononanoic acid (PFNA), perfluorodecanoic acid (PFDA), 2,3,3,3-tetrafluoro-2-(heptafluoropropoxy)propanoate (Gen X), perfluorooctanesulfonic acid, perfluorohexanesulfonic acid (PFHxS), and perfluorobutanesulfonic acid (PFBS) were obtained

111 from Accustandard, Inc (New Haven, CT). PFAS solutions in PBS were stored at room
112 temperature in polypropylene containers.
113 *Equilibrium Dialysis.* Samples were prepared in a rapid equilibrium dialysis device (RED;
114 Thermo Fisher, Waltham, MA) such that the final concentrations of each mixture would contain
115 10 μM bovine serum albumin (BSA) with either 10 μM, 1 μM, or 20 μM PFAS in phosphate
116 buffered saline (PBS). These samples were incubated for one hour at 37°C prior to
117 experimentation. The RED procedure was followed as described previously and as recommended
118 by the manufacturer (Gao et al., 2019; Waters et al., 2008). Controls of 10 μM of each PFAS
119 were also added to the plate to account for PFAS adsorption onto the membrane or sides of the
120 chamber. After four hours of incubation at 37°C under constant shaking, samples were collected
121 from both sides. Samples from the buffer side, containing no protein, were prepared for analysis
122 by liquid chromatography/mass spectrometry (LC/MS). Details of the full LC/MS procedure and
123 association constant analysis can be found in the Supplementary Information.
124 The fraction of bound PFAS was determined by mass balance as $f = ([\text{PFAS}]_{\text{initial}} -$
125 $[\text{PFAS}]_{\text{unbound}})/[\text{PFAS}]_{\text{initial}}$ where $[\text{PFAS}]_{\text{initial}} - [\text{PFAS}]_{\text{unbound}} = [\text{PFAS}]_{\text{bound}}$. From f, the
126 protein/water partition coefficient, K_{PW} (g bound PFAS mL^{-1} BSA)/(g free PFAS mL^{-1} water),
127 was determined as

128 $$K_{PW} = \frac{f}{\rho_P [P](1-f)} \qquad (1)$$

129 where ρ_P is the specific volume of the protein (0.733 mL g^{-1}) and [P] is the total BSA
130 concentration (10 μM or 6.6×10^{-3} g mL^{-1}) (Bischel et al., 2011). The association constant, K_a (M^{-1}),
131 was calculated as (Allendorf et al., 2019)

132 $$K_a = \frac{[PFAS]_{bound}}{([P] - [PFAS]_{bound})[PFAS]_{unbound}} \qquad (2)$$

where the term ([P] – $[PFAS]_{bound}$) represents the residual unbound BSA protein assuming 1:1 molar binding.

Fluorescence Quenching. Quenching experiments were conducted using a PerkinElmer LS 55 Fluorescence Spectrophotometer with a 150 W xenon discharge lamp. The temperature was set to 25°C, 30°C, 35°C, or 40°C using a PerkinElmer PTP-1 Peltier Temperature Programmer. The excitation wavelength was set to 295 nm, data was collected from an emission range of 300 nm to 500 nm at a rate of 100 nm/min, and the slit widths for both the emission and excitation were set to 6 nm.

A solution of BSA (2 mL) was added to a 1 cm quartz cuvette (Starna Cells, Atascadero, CA) and the fluorescence spectrum of BSA alone was measured to provide a baseline. Aliquots of PFAS stock solutions were added incrementally to achieve the desired concentration range. A linear calibration curve of BSA fluorescence intensity over a range of concentrations was used to correct for dilution of BSA. The quenching analyses performed herein were based on the emission intensity at a wavelength of 349 nm, which was the wavelength for maximum emission intensity for BSA alone.

RESULTS AND DISCUSSION

PFAS binding by equilibrium dialysis

Equilibrium dialysis provides a direct measure of PFAS-protein binding through specific and non-specific interactions, and a comparative basis for fluorescence quenching-based association constants. The fraction of bound PFAS f at 37°C, the resulting protein/water partition coefficient K_{PW}, and the calculated association constants K_a are reported in Table 1. In addition

to representing physiological temperature, 37°C was used in accordance with reported protocols for protein binding determined by equilibrium dialysis.

Table 1. Equilibrium dialysis results for PFAS-BSA binding at 37°C.

PFAS	***f*[a]**	***K*$_{PW}$ (10^5)[a]**	***K*$_a$ (10^5 M^{-1})[a]**	***K*$_a$ (*10^5 M^{-1}*)[b]**
PFOA	0.755 (0.038)	0.66 (0.13)	3.77 (0.80)	*11 (1.1)*
PFNA	0.975 (0.005)	8.52 (1.62)	44.05 (8.37)	*14 (2.2)*
PFDA	0.983 (0.004)	12.66 (3.23)	61.62 (15.72)	*36 (3.1)*
PFBS[c]	0.249 (0.064)	0.07 (0.02)	0.93 (0.55)	*1.1 (0.28)*
PFHxS	0.842 (0.008)	1.11 (0.06)	6.48 (0.39)	*44 (3.5)*
PFOS	0.942 (0.004)	3.39 (0.27)	17.99 (1.44)	*32 (4.9)*
Gen X[c]	0.265 (0.006)	0.07 (0.002)	0.65 (0.04)	*0.23 (0.05)*

[a]Standard error shown in parentheses

[b]Reported by Allendorf et al. (2019)

[c]K_{PW} and K_a determined at a PFAS:BSA molar ratio of 2:1. All other values are determined at a 0.1:1 molar ratio (Additional details in the Supplemental Information).

The values for the fraction of bound PFAS, *f*, and the resulting K_{PW} values obtained in this work are in agreement with Bischel et al (2011) for the longer compounds (PFNA, PFDA, and PFOS) but not for the shorter compounds where *f* values ≥0.99 were reported for PFOA, PFBS, and PFHxS. The *f* values for these shorter compounds fall between those reported by Bischel et al. (2011) and Allendorf et al. (2019), where low bound fractions were observed for PFOA and PFBS ($f = 0.44$), and PFHxS ($f = 0.62$). In this work, *f* increased with the number of fluorinated carbons from $C_{4,F}$ to $C_{9,F}$. There was no apparent evidence for longer compounds adopting a helical structure that would result in maximum K_{PW} values at $C_{6,F}$ with decreases in K_{PW} above $C_{7,F}$ (Bischel et al., 2011).

A positive correlation was observed between the association constants and the logarithm of the octanol-water partition coefficient, log K_{ow}, for non-ionic (associated; obtained from Pubmed; Figure 1A) and ionic (dissociated at pH 7.4; calculated using Marvin Sketch; Figure 1B) PFAS species, in agreement with values reported previously using PFAS chain length as a proxy for hydrophobicity (Table 1) (Allendorf et al., 2019). The PFCA correlation includes GenX, suggesting that binding of this alternative PFAS based on hydrophobicity is similar to the linear PFCA. Log K_{ow} correlations are used to examine quantitative structure-activity relationships (QSAR) governing ligand binding to proteins, with the log K_{ow} coefficient reflecting the strength of hydrophobic binding and depth of insertion into the protein structure (Hansch and Klein, 1986). A coefficient ≥ 1 indicates a strong dependence on hydrophobicity and deep insertion upon binding, which was observed for PFCA and PFSA. Larger log K_{ow} coefficients were determined for PFCA, suggesting a stronger dependence on hydrophobicity.

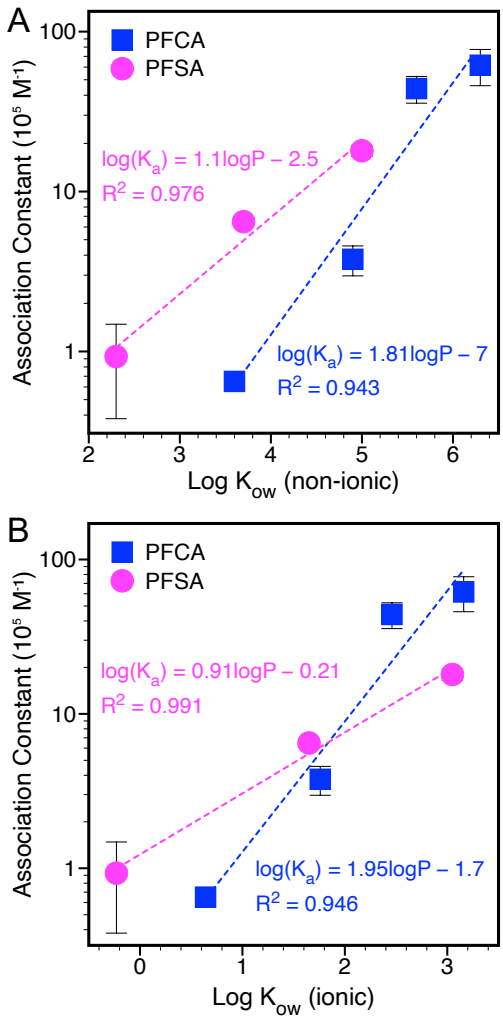

185

186 Figure 1. PFAS-BSA association constant determined by equilibrium dialysis as a function of the
187 logarithm of the octanol-water partition coefficient, log K_{ow}, for (A) non-ionic (associated;
188 obtained from Pubmed) and (B) ionic (dissociated at pH 7.4; calculated using Marvin Sketch)
189 PFAS species. Standard error bars not observed are smaller than the symbols. K_a in the fitted
190 equations has units of 10^5 M^{-1}.

191

192 **PFAS binding by fluorescence quenching**

193 In contrast to equilibrium dialysis measurements, fluorescence quenching-based
194 measurements are based on PFAS binding to specific sites on BSA containing tryptophan (Trp)

residues. The extent of fluorescence quenching can be directly related to PFAS concentration through the Stern-Volmer equation, which has been reported for PFAS-BSA binding (Bischel et al., 2011, 2010; Chen et al., 2015; MacManus-Spencer et al., 2010; Qin et al., 2010). The Stern-Volmer equation is written as (Lakowicz, 2006)

$$\frac{F_0}{F} - 1 = K_{SV}[Q] \qquad (3)$$

where F is the fluorescence emission intensity at a specified wavelength (349 nm) of the protein in the presence of the quencher, F_0 is the fluorescence emission intensity of the protein in the absence of the quencher, K_{SV} is the Stern-Volmer association constant, and $[Q]$ is the concentration of the unbound quencher, $[\text{PFAS}]_{\text{unbound}}$. In terms of BSA and PFAS, K_{SV} is the degree of association between the quencher and the protein at equilibrium

$$[PFAS] + [BSA] \rightleftharpoons [BSA - PFAS] \qquad (4)$$

$$K_{SV} \approx K_{eq} = \frac{[BSA - PFAS]}{[PFAS][BSA]} \qquad (5)$$

where [BSA-PFAS] is the concentration of the bound complex. The Stern-Volmer equation is based on the following assumptions (Eftink and Ghiron, 1981; Lakowicz, 2006): (i) The concentration of the quencher is large relative to protein concentration such that $[Q]_{\text{total}}$ (or $[\text{PFAS}]_{\text{total}}$) can be substituted for $[Q]$ (or $[\text{PFAS}]_{\text{unbound}}$), (ii) the protein-quencher complex is nonfluorescent, and (iii) binding is noncooperative.

Exemplary spectra and Stern-Volmer plots are shown in the Figures S2 and S3, respectively. With the exception of PFNA, equation 3 yielded a linear curve suggesting a static quenching process where the BSA-PFAS complex is non-fluorescent. However, fitted K_{SV} values over [PFAS] from 0 to 6.8 μM did not change appreciably over the temperature range examined (Figure 2A; Table S2), in contrast with reported studies showing a strong temperature

dependence indicative of enthalpic binding. This may reflect a more dominant entropic contribution as previously shown using ^{19}F-NMR (Fedorenko et al., 2021) or an apparent combined static and dynamic quenching process, where elevated temperatures increase the diffusivity of binding ligands and thus the collision frequency with the binding site. Compared to previous studies, the K_{SV} values obtained in this work at 25°C are on the same order of magnitude for PFOA and PFOS at reported temperatures ranging from 21°C to 27°C (Chen et al., 2015; Li et al., 2010; Qin et al., 2010).

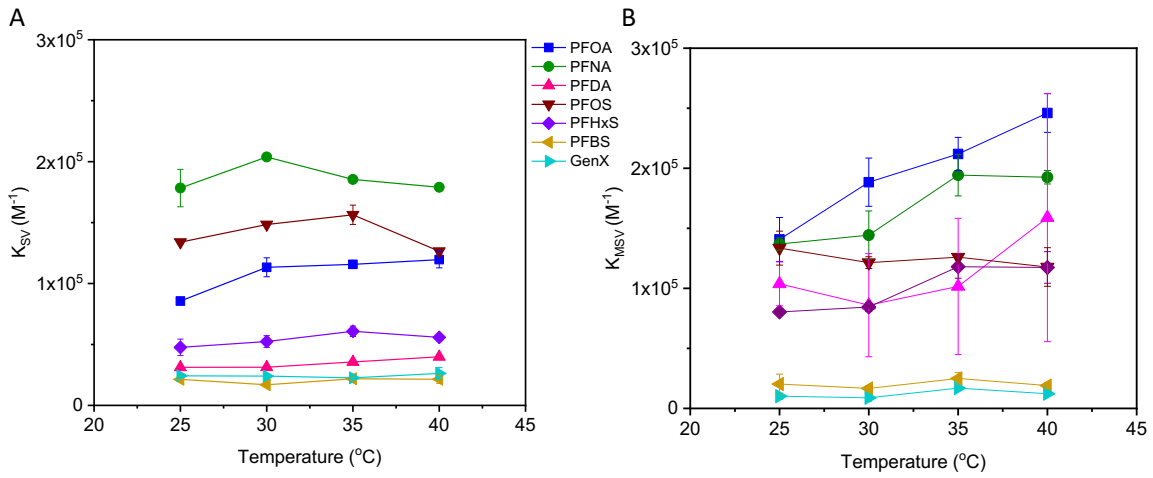

Figure 2. A) Stern-Volmer (K_{SV}; equation 3, Figure S3) and B) modified Stern-Volmer (K_{MSV}; equation 6, Figure S4) association constants for PFAS binding to BSA as a function of temperature. Standard error bars shown are based on two independent measurements.

The first limiting assumption of the Stern-Volmer equation is that $[PFAS]_{total} \approx [PFAS]_{unbound}$. To test this assumption, $[PFAS]_{total}$ was increased ten-fold and [BSA] was held constant. Results for fluorescence quenching decayed exponentially with increasing [PFAS], displaying a plateau at high [PFAS]. In this case, the modified Stern-Volmer equation was

required to account for saturation by incorporating a fractional accessibility term, f_a, of the PFAS to the quenching site (Chen and Guo, 2009; Qin et al., 2010)

$$\frac{F_0}{F_0 - F} = \frac{1}{f_a K_{MSV}[Q]} + \frac{1}{f_a} \qquad (6)$$

where K_{MSV} is the modified Stern-Volmer association constant. Equation 6 accounts for downward curvature in Stern-Volmer plots and assumes that, as [Q] ➛ ∞, only the inaccessible fluorescent amino acid residues can fluoresce. Thus, it allows for two types of fluorescent residues in a protein—those accessible to the quencher and those not accessible to the quencher—with no allowance for a partially accessible fluorophore or for binding cooperativity (Lakowicz, 2006). For BSA this involves PFAS binding near Trp-214 and Trp-134, with one of these sites being inaccessible. The modified Stern-Volmer equation was applied over [PFAS] ranging from 14.7 to 68.2 μM for PFCAs and 7.4 to 74.2 μM or 35.7 to 74.2 μM for PFSAs. Data obtained below these lower [PFAS] limits led to poor fits.

Fitted K_{MSV} were similar to K_{SV} for many of the PFAS examined (Figure 2, Tables S2 and S3), which implies that the assumption $[PFAS]_{total} \approx [PFAS]_{unbound}$ is reasonable for the Stern-Volmer model and that 'fractional accessibility' accounts for saturation at high [PFAS] in the modified Stern-Volmer model. However, the trends in the association constants with PFAS size were different with the exception of the two smallest PFAS, GenX and PFBS. These trends are shown below for 25°C with the largest PFAS, PFDA, in bold and the sulfonates underlined to distinguish them.

K_{SV}: PFNA > <u>PFOS</u> > PFOA > <u>PFHxS</u> > **PFDA** > GenX ≈ <u>PFBS</u>

K_{MSV}: PFOA > PFNA > <u>PFOS</u> > **PFDA** ≈ <u>PFHxS</u> > <u>PFBS</u> ≈ GenX

The f_a values (Table S3), ranged from approximately 0.5 to 0.7, with PFBS being the exception (~0.3). Mechanistically, this means that the binding sites with fluorescent Trp residues

257 are less accessible to PFBS binding. Being the smallest and most water soluble PFAS examined,
258 PFBS ($C_{n,F}$ = 4) may have lacked the hydrophobicity needed to insert into the hydrophobic,
259 tryptophan-containing regions of BSA. Interestingly, this argument does not apply to GenX ($C_{n,F}$
260 = 5), which showed similarly small K_{MSV} values with f_a values that were two-fold higher than
261 PFBS. Despite GenX having access to the binding sites, the affinity between GenX and the
262 binding site was low. This may be due to the non-linear structure where the CF_3 group near the
263 carboxylic acid headgroup sterically hindered binding.
264 The third model applied to the fluorescence quenching data – the Hill equation – also
265 accounts for the residual fluorescence upon saturation, F_{res}, but does not ascribe F_{res} to
266 fractional accessibility. The model applied is based on the Hill approximation proposed by
267 Hebert et al for PFAS-protein binding (Hebert and MacManus-Spencer, 2010)

268 $$\frac{F_0 - F}{F_0 - F_{res}} = \left[\frac{(K_{Hill}[Q])^{n_{Hill}}}{1 + (K_{Hill}[Q])^{n_{Hill}}}\right] \qquad (7)$$

269 where K_{Hill} and n_{Hill} are the Hill binding constant and coefficient, respectively. At high [PFAS]
270 relative to [BSA], this model accurately reflects the quenching conditions, which are dependent
271 upon the change in protein conformation with the type and concentration of PFAS (Hebert and
272 MacManus-Spencer, 2010). This dependence is described by n_{Hill}, which accounts for binding
273 cooperativity. Hill coefficients greater than 1, $n_{Hill} > 1$, denote positive binding cooperativity,
274 $n_{Hill} < 1$ denote negative binding cooperativity, and $n_{Hill} = 1$ denote noncooperative binding.
275 Unlike the Stern-Volmer and modified Stern-Volmer models where data sets were truncated to
276 accommodate the models, excellent fits were obtained for the Hill model over the entire
277 concentration range examined.
278 Comparisons between K_{Hill}, K_{MSV} and K_{SV} are shown in Figure 3 at the four temperatures
279 examined (data presented in Table S3). Overall, the association constants based on K_{Hill} were

similar to or greater than that for K_{MSV} and K_{SV}; or alternatively, the Stern-Volmer models underestimated PFAS-BSA binding compared to the Hill model. This was particularly true for the most hydrophobic carboxylic acids, PFOA, PFNA, and PFDA. There was comparatively better agreement between K_{Hill}, K_{MSV} and K_{SV} with the sulfonic acids.

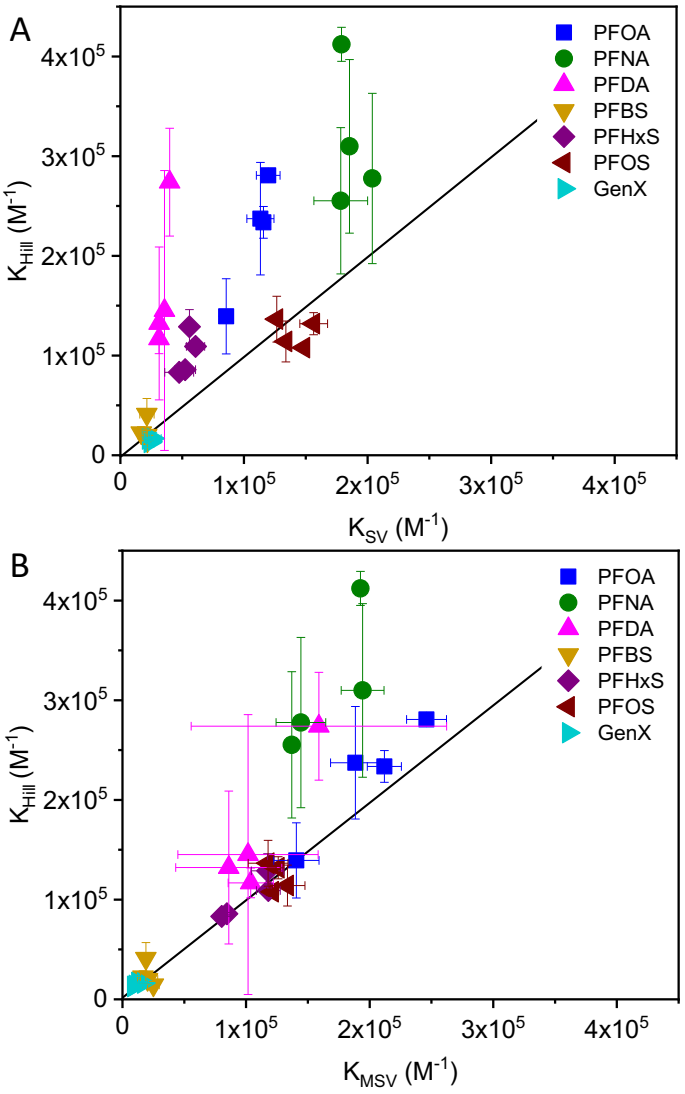

Figure 3. Comparison of PFAS-BSA association constants determined by fluorescence quenching from the Hill equation (K_{Hill}) to those determined using the (A) Stern-Volmer (K_{SV}) and (B) modified Stern-Volmer (K_{MSV}) equations. The data points for each PFAS were obtained

288 at temperatures of 25°C, 30°C, 35°C, and 40°C (data shown in Table S3). The solid lines
289 represent the condition where the association constants are equal.
290
291 Additional insight can be gained by analyzing the binding cooperativity described by
292 n_{Hill} as a function of the number of fluorinated carbons (Figure 4). Results shown at 25°C and
293 35°C depict two regions – negative cooperativity or noncooperative/positive cooperativity – that
294 are independent of temperature. Negative binding cooperativity ($n_{Hill} < 1$) was observed for
295 small (PFBS, $C_{n,F} = 4$) and large (PFDA, $C_{n,F} = 9$) PFAS, while noncooperative (GenX, PFNA)
296 or positive binding cooperativity (PFHxS, PFOA, PFOS) was observed for PFAS with $C_{n,F} = 5$ to
297 8 ($n_{Hill} \geq 1$). The trend in binding cooperativity with $C_{n,F}$ may reflect the ability for intermediate
298 PFAS to 'fit within' and bind to the hydrophobic regions containing Trp, leading to
299 conformational changes within the protein that further increases binding affinity (Bischel et al.,
300 2011).

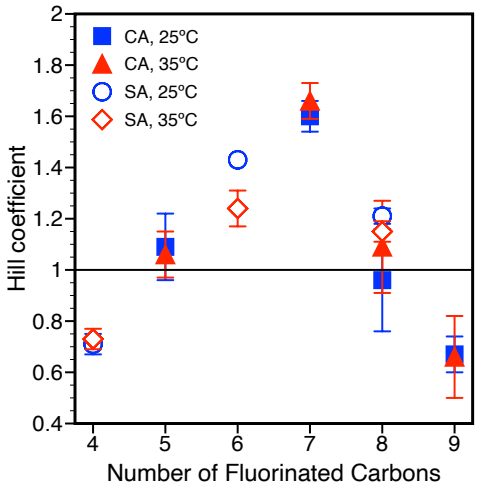

301
302 Figure 4. Hill coefficient, obtained from the Hill model fitting (equation 7), describing PFAS-
303 BSA binding cooperativity. Standard error bars shown are based on three independent

304 measurements for PFCAs and two independent measurements for PFSAs. PFCA and PFSA are
305 abbreviated as CA and SA, respectively.
306
307 To further describe the trends in binding across the range of PFAS, the association
308 constants obtained via fluorescence quenching were compared to molecular descriptors. Results
309 for K_a versus the number of fluorinated carbons (Figure 5A) agree with previous work showing
310 that PFOA and PFOS preferentially bind to a hydrophobic cavity within a serum albumin protein
311 (Chen and Guo, 2009; Salvalaglio et al., 2010). However, the number of fluorinated carbons is
312 not an adequate proxy for molecular size. PFNA showed the highest association constant, higher
313 than PFOS, despite having the same number of fluorinated carbons. An analysis of the van der
314 Waals volume, V_{vdW}, shows that PFOS ($C_{8,F}$) is larger than PFNA ($C_{8,F}$) and similar in size to
315 PFDA ($C_{9,F}$), which also showed a lower K_a compared to PFNA (Figure 5B). The importance of
316 steric hinderance is further denoted by PFOA ($C_{7,F}$), which is less hydrophobic than PFOS and
317 has a considerably smaller V_{vdW}, but similar association with BSA. The trends in K_a with V_{vdW}
318 are similar to those with the ionic log K_{ow} (Figure 5C), which takes into consideration the
319 headgroup charge, where the two largest PFAS, PFOS and PFDA, are also the most hydrophobic
320 yet exhibit a lower K_a than PFNA. This trend was not captured with the associated log K_{ow}
321 values (Figure 5D). Above an optimal size, described by V_{vdW}, the PFAS molecules no longer
322 'fit' into the same location on BSA regardless of their hydrophobicity.

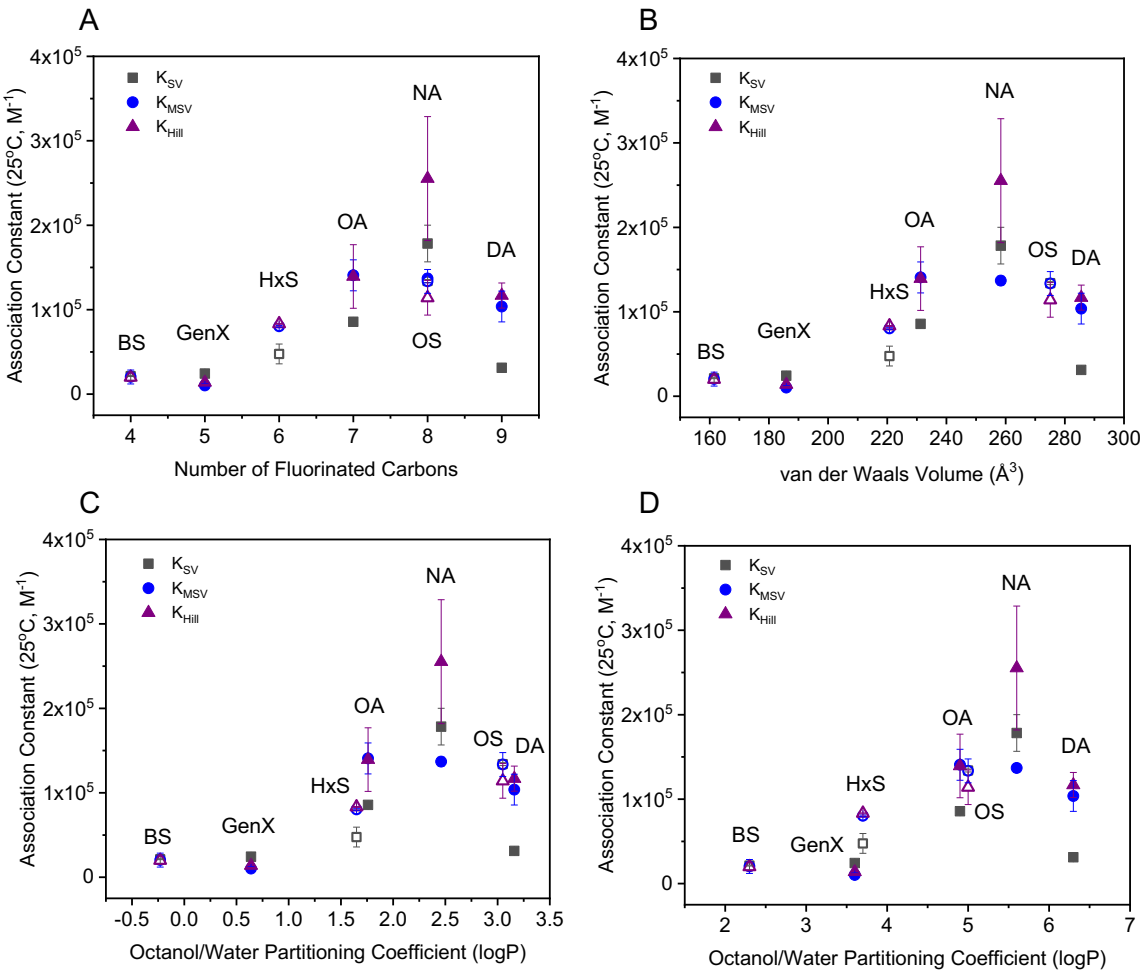

Figure 5. PFAS association constants determined by fluorescence quenching as a function of molecular descriptors: A) the number of fluorinated carbons, B) the calculated van der Waals volume, C) the logarithm of the ionic the octanol-water partitioning coefficient, or ionic log K_{ow}, calculated at pH 7.4, and D) the calculated logarithm of the octanol-water partitioning coefficient or log K_{ow}. Closed symbols correspond with PFCA and open symbols PFSA.

The hydrophobic nature of the PFAS-protein interactions can be explored further by evaluating the wavelength shift in the fluorescence spectra (Figure S5), consistent with previous studies of both BSA and HSA (Liu et al., 2017; Qin et al., 2010; Wu et al., 2009). A shift in the

wavelength associated with maximum fluorescence emission indicates a change in the solvent environment surrounding the fluorescent Trp residues. PFBS and GenX do not show marked shifts in emission wavelength, consistent with low binding affinity within the hydrophobic cavity of BSA and/or their inability to dehydrate the cavity and cause local decreases in solvent polarity. For all other PFAS, the blue shift indicates that PFAS binding created a more hydrophobic environment as the conformation of the protein changes and bound water molecules are displaced by the PFAS (Vivian and Callis, 2001). The extent of wavelength shift roughly correlates with PFAS hydrophobicity. The maximum shifts occur for PFNA (-13 nm) for the carboxylates and PFHxS (-10 nm) for the sulfonates. The shift was not as great for the larger PFDA (-10 nm) or PFOS (-7 nm), supporting the concept that these molecules do not fit as well within the cavity, which has been reported for PFDA but not PFOS (Bischel et al., 2010; Macmanus-spencer et al., 2010).

Mechanistic insight comparing fluorescence quenching and equilibrium dialysis

The difference between the two experimental methods presented here is that fluorescence quenching reflects PFAS binding within the hydrophobic cavity of BSA, while equilibrium dialysis reflects all binding. Comparing these results can shed more light on the interaction of different PFAS with BSA. For PFDA (Figure 6), the K_a from equilibrium dialysis is an order of magnitude higher than K_a values determined by fluorescence quenching. As PFDA is the largest molecule studied (Figure 5B) based on V_{vdW}, size exclusion from the hydrophobic pockets may make binding to the surface more energetically favorable. For sulfonates, PFOS shows a similar trend. Although PFOS and PFNA have the same number of fluorinated carbons, PFNA has a higher association constant than PFOS.

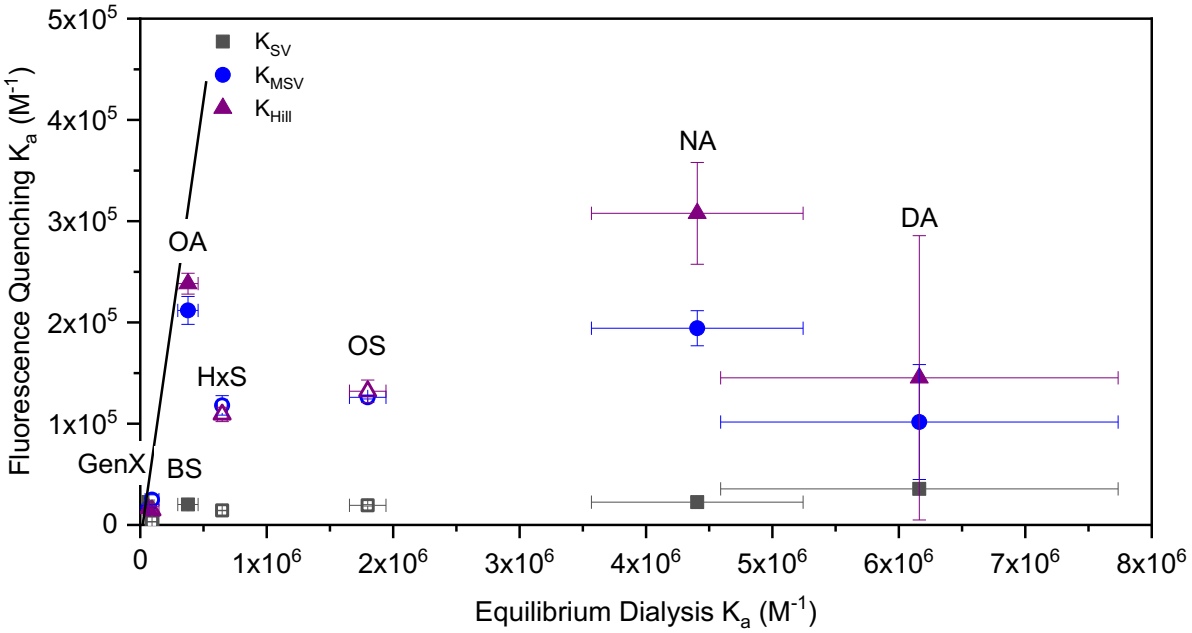

Figure 6. A comparison of association constants determined at 35°C by fluorescence quenching and equilibrium dialysis. The solid lines represent the condition where the association constants are equal. Closed symbols correspond with PFCA and open symbols PFSA.

Based on the comparison in Figure 6, protein binding based on the Hill equation, which accounts for binding cooperativity, is in closer agreement with the 'true' extent of binding based on equilibrium dialysis, particularly for the more hydrophobic PFAS. However, the results clearly demonstrate that both approaches should be combined to gain a mechanistic understanding of PFAS binding as a function of their physicochemical properties.

The importance of understanding the effect of physicochemical properties on protein binding becomes more apparent as industry producers move toward using shorter chain length PFAS. However, shorter chains do not necessarily result in lower protein binding affinities than longer chain PFAS. Our work shows, based on both experimental techniques, that PFHxS binds

to BSA with similar affinity as PFOS. This is significant to exposure assessment and health risks as albumin has been shown to be the major carrier of PFAS in human blood (Forsthuber et al., 2020). As more PFASs are developed as alternatives to legacy compounds, there is a pressing need to continue to rigorously assess protein binding and identify correlations with PFAS molecular properties. One way to accomplish this is through the link between log K_{ow} and degree of binding. For example, as log K_{ow} (hydrophobicity) increases for the PFAS of $C_{8,F}$ and smaller in this study, the degree of binding to BSA increases. As is shown with PFDA ($C_{9,F}$), this model parameter should be coupled with Van der Waals volume to account for steric hinderance to binding.

CONCLUSIONS AND IMPLICATIONS

With albumin being a major protein carrier for PFAS *in vivo*, accurate protein binding constants and mechanistic insight into binding are imperative to guide bioaccumulation models and physiologically based pharmacokinetic/pharmacodynamic (PBPK/PBPD) models. In this work, a systematic analysis of fluorescence-based protein binding models was conducted for an expanded range of PFAS and compared to equilibrium dialysis experiments. Both experimental methods provide valuable and complimentary insight into PFAS- BSA binding. While fluorescence quenching focuses on the hydrophobic pocket of the protein, equilibrium dialysis reports all types of binding, whether in specific locations or to the surface. By critically examining the differences between the equilibrium dialysis and fluorescence quenching, we can gain insight into binding mechanisms, especially for those PFAS-serum protein interactions that have not yet been characterized by crystal structure or other methods.

Fluorescence quenching has been used to evaluate PFAS binding to serum albumin proteins but there is no clear guidance on the applicability or limitations of the three models discussed in this work: the Stern-Volmer model, the modified Stern-Volmer model, and the Hill equation. By limiting analysis to one of these methods, valuable insight about binding cooperativity and fractional accessibility to binding sites may not be gained. Combining models affords another layer of mechanistic insight. As with any model, understanding the assumptions and limitations is vital to interpretation of the underlying mechanisms.

In addition, the trend in association constants with respect to physicochemical properties suggests that both hydrophobic and steric effects play a role in degree of binding to serum albumins. As models are developed to predict transport of PFAS through the human body, these intrinsic physicochemical properties are extremely useful. Additional work must be completed in this area, especially for PFAS of different structures than those studied herein.

ACKNOWLEDGEMENTS

This work was funded by the National Institute of Environmental Health Science Sources, Transport, Exposure & Effects of PFASs (STEEP) Superfund Research Program under grant P42ES027706. STEEP is a partnership of the University of Rhode Island, the Harvard T.H. Chan School of Public Health, and the Silent Spring Institute.

411 **REFERENCES**

412 Ahrens, L., Bundschuh, M., 2014. Fate and effects of poly- and perfluoroalkyl substances in the
413 aquatic environment: A review. Environ. Toxicol. Chem. 33, 1921–1929.
414 https://doi.org/10.1002/etc.2663

415 Allendorf, F., Berger, U., Goss, K.U., Ulrich, N., 2019. Partition coefficients of four
416 perfluoroalkyl acid alternatives between bovine serum albumin (BSA) and water in
417 comparison to ten classical perfluoroalkyl acids. Environ. Sci. Process. Impacts 21, 1852–
418 1863. https://doi.org/10.1039/c9em00290a

419 Bischel, H.N., MacManus-Spencer, L.A., Luthy, R.G., 2010. Noncovalent Interactions of Long-
420 Chain Perfluoroalkyl Acids with Serum Albumin. Environ. Sci. Technol. 44, 5263–5269.
421 https://doi.org/10.1021/es101334s

422 Bischel, H.N., MacManus-Spencer, L.A., Zhang, C., Luthy, R.G., 2011. Strong associations of
423 short-chain perfluoroalkyl acids with serum albumin and investigation of binding
424 mechanisms. Environ. Toxicol. Chem. 30, 2423–2430. https://doi.org/10.1002/etc.647

425 Boston, C.M., Banacos, N., Heiger-Bernays, W., 2019. Per- and Polyfluoroalkyl Substances: A
426 National Priority for Safe Drinking Water. Public Health Rep. 134, 112–117.
427 https://doi.org/10.1177/0033354919826567

428 Cardenas, A., Gold, D.R., Hauser, R., Kleinman, K.P., Hivert, M.-F., Calafat, A.M., Ye, X.,
429 Webster, T.F., Horton, E.S., Oken, E., 2017. Plasma Concentrations of Per- and
430 Polyfluoroalkyl Substances at Baseline and Associations with Glycemic Indicators and
431 Diabetes Incidence among High-Risk Adults in the Diabetes Prevention Program Trial.
432 Environ. Health Perspect. 125, 107001. https://doi.org/10.1289/EHP1612

433 Chen, H., He, P., Rao, H., Wang, F., Liu, H., Yao, J., 2015. Systematic investigation of the toxic

mechanism of PFOA and PFOS on bovine serum albumin by spectroscopic and molecular modeling. Chemosphere 129, 217–224. https://doi.org/10.1016/j.chemosphere.2014.11.040

Chen, Y.M., Guo, L.H., 2009. Fluorescence study on site-specific binding of perfluoroalkyl acids to human serum albumin. Arch. Toxicol. 83, 255–261. https://doi.org/10.1007/s00204-008-0359-x

Cheng, W., Ng, C.A., 2018. Predicting Relative Protein Affinity of Novel Per- and Polyfluoroalkyl Substances (PFASs) by An Efficient Molecular Dynamics Approach. Environ. Sci. Technol. 52, 7972–7980. https://doi.org/10.1021/acs.est.8b01268

Dassuncao, C., Hu, X.C., Nielsen, F., Weihe, P., Grandjean, P., Sunderland, E.M., 2018. Shifting Global Exposures to Poly- and Perfluoroalkyl Substances (PFASs) Evident in Longitudinal Birth Cohorts from a Seafood-Consuming Population. Environ. Sci. Technol. 52, 3738–3747. https://doi.org/10.1021/acs.est.7b06044

Domingo, J.L., Nadal, M., 2017. Per- and polyfluoroalkyl substances (PFASs) in food and human dietary intake: A review of the recent scientific literature. J. Agric. Food Chem. 65, 533–543. https://doi.org/10.1021/acs.jafc.6b04683

Eftink, M.R., Ghiron, C.A., 1981. Fluorescence quenching studies with proteins. Anal. Biochem. 114, 199–227. https://doi.org/10.1016/0003-2697(81)90474-7

Fedorenko, M., Alesio, J., Fedorenko, A., Slitt, A., Bothun, G.D., 2021. Dominant entropic binding of perfluoroalkyl substances (PFASs) to albumin protein revealed by 19F NMR. Chemosphere 263, 128083. https://doi.org/10.1016/j.chemosphere.2020.128083

Forsthuber, M., Kaiser, A.M., Granitzer, S., Hassl, I., Hengstschläger, M., Stangl, H., Gundacker, C., 2020. Albumin is the major carrier protein for PFOS, PFOA, PFHxS, PFNA and PFDA in human plasma. Environ. Int. 137, 105324.

https://doi.org/10.1016/j.envint.2019.105324

Gao, K., Zhuang, T., Liu, X., Fu, Jianjie, Zhang, J., Fu, Jie, Wang, L., Zhang, A., Liang, Y., Song, M., Jiang, G., 2019. Prenatal Exposure to Per- and Polyfluoroalkyl Substances (PFASs) and Association between the Placental Transfer Efficiencies and Dissociation Constant of Serum Proteins–PFAS Complexes. Environ. Sci. Technol. 53, 6529–6538. https://doi.org/10.1021/acs.est.9b00715

Gitlin, D., Klinenberg, J.R., Hughes, W.L., 1958. Site of Catabolism of Serum Albumin. Nature 181, 1064–1065.

Grandjean, P., Budtz-Jørgensen, E., 2013. Immunotoxicity of perfluorinated alkylates: calculation of benchmark doses based on serum concentrations in children. Environ. Heal. 12, 35. https://doi.org/10.1186/1476-069X-12-35

Hansch, C., Klein, T.E., 1986. Molecular graphics and QSAR in the study of enzyme-ligand interactions. On the definition of bioreceptors. Acc. Chem. Res. 19, 392–400. https://doi.org/10.1021/ar00132a003

Hartman, T.J., Calafat, A.M., Holmes, A.K., Marcus, M., Northstone, K., Flanders, W.D., Kato, K., Taylor, E. V., 2017. Prenatal Exposure to Perfluoroalkyl Substances and Body Fatness in Girls. Child. Obes. 13, 222–230. https://doi.org/10.1089/chi.2016.0126

Hebert, P.C., MacManus-Spencer, L.A., 2010. Development of a Fluorescence Model for the Binding of Medium- to Long-Chain Perfluoroalkyl Acids to Human Serum Albumin Through a Mechanistic Evaluation of Spectroscopic Evidence. Anal. Chem. 82, 6463–6471. https://doi.org/10.1021/ac100721e

Hu, X.C., Andrews, D.Q., Lindstrom, A.B., Bruton, T.A., Schaider, L.A., Grandjean, P., Lohmann, R., Carignan, C.C., Blum, A., Balan, S.A., Higgins, C.P., Sunderland, E.M.,

2016. Detection of Poly- and Perfluoroalkyl Substances (PFASs) in U.S. Drinking Water Linked to Industrial Sites, Military Fire Training Areas, and Wastewater Treatment Plants. Environ. Sci. Technol. Lett. 3, 344–350. https://doi.org/10.1021/acs.estlett.6b00260

Lakowicz, J.R., 2006. Principles of fluorescence spectroscopy, 3rd Edition, Joseph R. Lakowicz, editor, Principles of fluorescence spectroscopy, Springer, New York, USA, 3rd edn, 2006. https://doi.org/10.1007/978-0-387-46312-4

Li, L., Song, G.W., Xu, Z.S., 2010. Study on the interaction between bovine serum albumin and potassium perfluoro octane sulfonate. J. Dispers. Sci. Technol. 31, 1547–1551. https://doi.org/10.1080/01932690903294139

Liu, Y., Cao, Z., Zong, W., Liu, R., 2017. Interaction rule and mechanism of perfluoroalkyl sulfonates containing different carbon chains with human serum albumin. RSC Adv. 7, 24781–24788. https://doi.org/10.1039/c7ra02963b

Macmanus-spencer, L. a, Tse, M.L., Hebert, P.C., Bischel, H.N., Luthy, R.G., 2010. Binding of Perfluorocarboxylates to Serum Albumin : A Comparison of Analytical Methods quantitative information about PFCA - albumin interac-. Anal. Chem. 82, 974–981.

MacManus-Spencer, L.A., Tse, M.L., Hebert, P.C., Bischel, H.N., Luthy, R.G., 2010. Binding of Perfluorocarboxylates to Serum Albumin: A Comparison of Analytical Methods. Anal. Chem. 82, 974–981. https://doi.org/10.1021/ac902238u

Ng, C.A., Hungerbühler, K., 2014. Bioaccumulation of perfluorinated alkyl acids: Observations and models. Environ. Sci. Technol. 48, 4637–4648. https://doi.org/10.1021/es404008g

Qin, P., Liu, R., Pan, X., Fang, X., Mou, Y., 2010. Impact of Carbon Chain Length on Binding of Perfluoroalkyl Acids to Bovine Serum Albumin Determined by Spectroscopic Methods. J. Agric. Food Chem. 58, 5561–5567. https://doi.org/10.1021/jf100412q

Ross, I., McDonough, J., Miles, J., Storch, P., Thelakkat Kochunarayanan, P., Kalve, E., Hurst, J., S. Dasgupta, S., Burdick, J., 2018. A review of emerging technologies for remediation of PFASs. Remediat. J. 28, 101–126. https://doi.org/10.1002/rem.21553

Salvalaglio, M., Muscionico, I., Cavallotti, C., 2010. Determination of Energies and Sites of Binding of PFOA and PFOS to Human Serum Albumin. J. Phys. Chem. B 114, 14860–14874. https://doi.org/10.1021/jp106584b

Steinhardt, J., Krijn, J., Leidy, J.G., 1971. Differences between bovine and human serum albumins. Binding isotherms, optical rotatory dispersion, viscosity, hydrogen ion titration, and fluorescence effects. Biochemistry 10, 4005–4015. https://doi.org/10.1021/bi00798a001

Vivian, J.T., Callis, P.R., 2001. Mechanisms of Tryptophan Fluorescence Shifts in Proteins. Biophys. J. 80, 2093–2109. https://doi.org/10.1016/S0006-3495(01)76183-8

Waters, N.J., Jones, R., Williams, G., Sohal, B., 2008. Validation of a Rapid Equilibrium Dialysis Approach for the Measurement of Plasma Protein Binding. J. Pharm. Sci. 97, 4586–4595. https://doi.org/10.1002/jps.21317

Wu, L.-L., Gao, H.-W., Gao, N.-Y., Chen, F.-F., Chen, L., 2009. Interaction of perfluorooctanoic acid with human serum albumin. BMC Struct. Biol. 9, 31. https://doi.org/10.1186/1472-6807-9-31

Xiao, F., Sasi, P.C., Yao, B., Kubátová, A., Golovko, S.A., Golovko, M.Y., Soli, D., 2020. Thermal Stability and Decomposition of Perfluoroalkyl Substances on Spent Granular Activated Carbon. Environ. Sci. Technol. Lett. 7, 343–350. https://doi.org/10.1021/acs.estlett.0c00114

Supplemental Information

Critical new insights into the binding of poly- and perfluoroalkyl substances (PFAS) to albumin protein

Jessica Alesio,[†] Angela Slitt,[‡] and Geoffrey D. Bothun*[,†]

[†]Department of Chemical Engineering, University of Rhode Island, Kingston, Rhode Island 02881, United States.

[‡]Department of Biomedical and Pharmaceutical Sciences, University of Rhode Island, Kingston, Rhode Island 02881, United States.

METHODS

LC-MS/MS System. The LC-MS/MS analysis is completed using the liquid chromatograph (Shimadzu) equipped with a C18 column (3µm, 2.1mm X 150mm; Phenomenex) coupled to mass spectrometer (Shimadzu) operating in negative mode.

LC Conditions. For the analysis, 10 µL of dialysate is injected on the LC column (40°C) and target compounds are eluted with mobile phase gradient (Table S1.1) consisted of 2 mM ammonium acetate in water and acetonitrile (flow rate 0.5 mL/min).

Table S1.1. Gradient Mobile Phase Program.

mobile phase / time (min)	A (%) - 2mM ammonium acetate in water	B (%) - 2mM ammonium acetate in acetonitrile
0.0	50	50
6.0	15	85
8.0	15	85

8.01	50	50
10.0	50	50

MS/MS Conditions. The triple quadrupole tandem mass spectrometer is operated in multiple reaction monitoring (MRM) mode using negative electrospray ionization (ESI-). Instrument parameters are shown in Table S1.2 and compound specific MS/MS parameters are summarized in S1.3. Values for collision energy are determined through instrument optimization.

Table S1.2. Mass spectrometer (MS) instrumental parameters.

Curtain Gas (CUR)	30
Collision Gas (CAD)	medium
IonSpray Voltage (IS)	-4500 V
Temperature (TEM)	400°C
Ion Source Gas 1 (GS1)	30
Ion Source Gas 2 (GS2)	30

Table S1.3 MS/MS Parameters of target PFAS.

Analyte	Type	MRM transitions	Collision Energy (V)
PFOA	Target	413 → 369; 169	11; 19
PFNA	Target	463 → 419; 219	10; 16
PFDA	Target	513 → 469; 219	11; 20
PFBS	Target	299 → 80; 99	34; 28
PFHxS	Target	399 → 80; 99	49; 43
PFOS	Target	499 → 80; 99	50; 44
Gen X	Target	347 → 169; 285	12; 20

Final PFAS concentrations from the dialysis experiment were determined by comparing to external standards of concentrations from 0.02 nM to 200 nM. All calibration curves had R^2

values above 0.99. The value of K_a was calculated as [PL]/([P]x[L]) with P being protein and L being ligand, as calculated in previous works (Allendorf et al., 2019). For all PFAS other than Gen X and PFBS, K_a was calculated by using the lowest PFAS to BSA ratio (0.1:1). In the cases of Gen X and PFBS, the small difference between initial and final concentration for this ratio led to the use of a ratio of 2:1 for more precise values.

RESULTS AND DISCUSSION

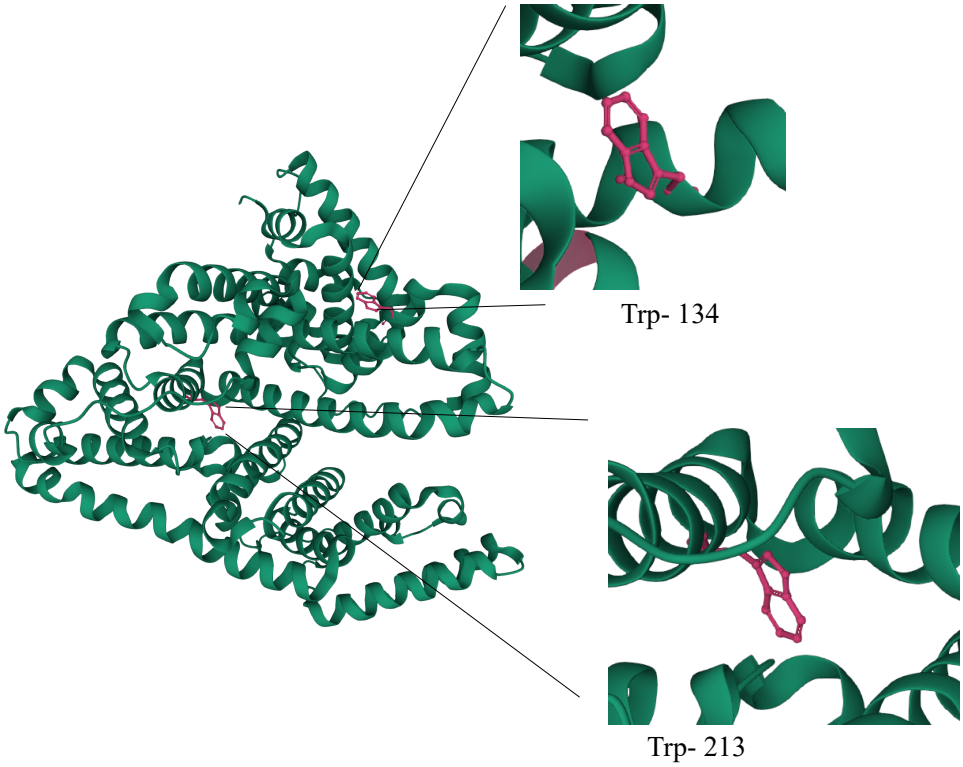

Figure S1. The structure of bovine serum albumin (BSA) with tryptophan residues shown in pink (Protein Data Bank Entry 3V03; Berman et al., 2002; Majorek et al., 2012; Sehnal et al., 2018). Trp-134 is more solvent-accessible while Trp-213 is located within the hydrophobic pocket of the protein.

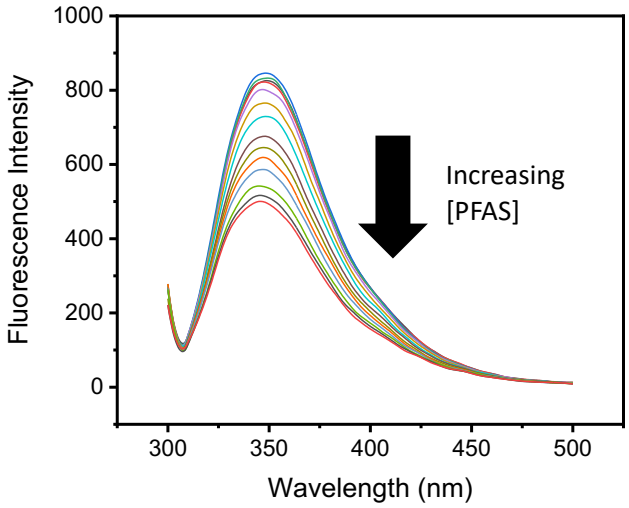

569

570 Figure S2. Representative fluorescence quenching plot for PFOA (0-6.8μM) added to a BSA

571 concentration of 1.25 μM at a temperature of 25°C. As the concentration of PFAS increases, the

572 fluorescence of BSA decreases, indicative of binding.

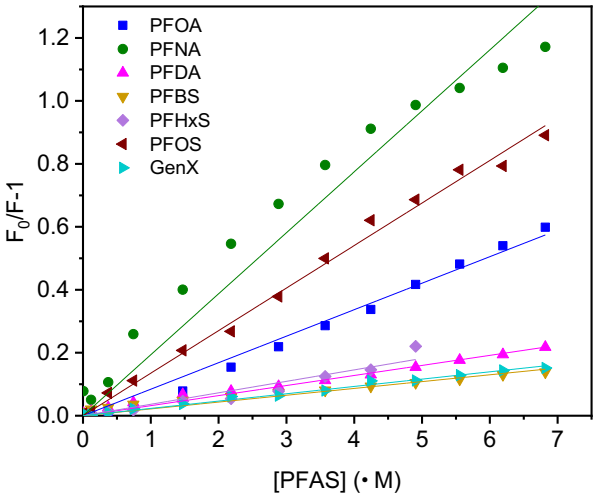

573

574 Figure S3. Representative Stern-Volmer plot with PFAS concentration ranging from 0 to 6.8 μM

575 and a BSA concentration of 1.25 μM at a temperature of 25°C. Values of R^2 were above 0.97 for

all PFAS other than PFBS at all temperatures studied. Values of R^2 for PFBS ranged from 0.92-0.99.

Table S2. Stern-Volmer Association Constants (K_{SV}) from fluorescence quenching experiments, [PFAS] = 0-6.8 μM, [BSA] = 1.25 μM.

PFAS	K_{SV} (10^5 M^{-1}) 25°C	K_{SV} (10^5 M^{-1}) 30°C	K_{SV} (10^5 M^{-1}) 35°C	K_{SV} (10^5 M^{-1}) 40°C
PFOA	0.85 (0.02)	1.13 (0.1)	1.16 (0.04)	1.20 (0.1)
PFNA	1.78 (0.22)	2.04 (0.03)	1.85 (0.01)	1.79 (0.07)
PFDA	0.31 (0.01)	0.31 (0.04)	0.36 (0.02)	0.40 (0.02)
PFBS	0.21 (0.01)	0.17 (0.02)	0.22 (0.03)	0.22 (0.06)
PFHxS	0.48 (0.12)	0.52 (0.08)	0.61 (0.07)	0.56 (0.03)
PFOS	1.34 (0.02)	1.48 (0.02)	1.56 (0.11)	1.26 (0.03)
Gen X	0.24 (0.01)	0.24 (0.03)	0.22 (0.02)	0.26 (0.07)

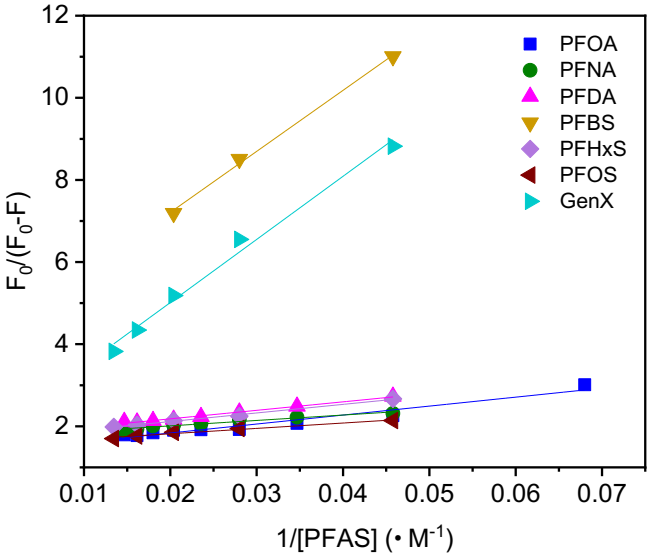

Figure S4. Representative modified Stern-Volmer plot with PFAS concentration ranging from 14.7 to 68.2 μM for PFCAs and 7.4 to 74.2 μM or 35.7 to 74.2 μM for PFSAs and a BSA concentration of 1.25 μM at a temperature of 25°C. Values of R^2 for all of these plots were

above 0.92 for PFCAs and above 0.95 for PFSAs at all temperatures studied. Inclusion of data in the ranges lower than reported led to deviations from linearity and poor fits.

Table S3. Modified Stern-Volmer Association Constants (K_{MSV}), fractional accessibility (f_a), Hill association constant (K_{Hill}), and number of Hill binding sites (n_{Hill}) from fluorescence quenching experiments, [PFCA] = 0-68.2 μM, [PFSA] = 0-74.2 μM, [BSA] = 1.25 μM. Standard error from duplicate measurements is shown in parenthesis.

PFAS	K_{MSV} (10^5 M^{-1})	f_a	K_{Hill} (10^5 M^{-1})	n_{Hill}
		25°C		
PFOA	1.41 (0.18)	0.61 (0.02)	1.39 (0.38)	1.60 (0.06)
PFNA	1.37 (0.05)	0.62 (0.03)	2.55 (0.73)	0.96 (0.20)
PFDA	1.04 (0.18)	0.60 (0.03)	1.17 (0.15)	0.67 (0.07)
PFBS	0.20 (0.08)	0.31 (0.08)	0.20 (0.05)	0.71 (0.04)
PFHxS	0.80 (0.01)	0.59 (0.002)	0.83 (0.01)	1.43 (0.00)
PFOS	1.33 (0.14)	0.64 (0.001)	1.14 (0.21)	1.21 (0.03
Gen X	0.10 (0.02)	0.59 (0.07)	0.14 (0.02)	1.09 (0.13)
		30°C		
PFOA	1.88 (0.20)	0.58 (0.02)	2.37 (0.57)	1.49 (0.17)
PFNA	1.44 (0.20)	0.63 (0.01)	2.78 (0.85)	1.10 (0.34)
PFDA	0.86 (0.43)	0.65 (0.04)	1.32 (0.77)	0.73 (0.23)
PFBS	0.16 (0.02)	0.26 (0.03)	0.23 (0.06)	0.91 (0.05)
PFHxS	0.84 (0.04)	0.56 (0.005)	0.86 (0.01)	1.58 (0.01)
PFOS	1.21 (0.05)	0.62 (0.01)	1.08 (0.02)	1.39 (0.14)
Gen X	0.09 (0.03)	0.67 (0.09)	0.13 (0.05)	1.19 (0.32)
		35°C		
PFOA	2.12 (0.14)	0.55 (0.01)	2.34 (0.16)	1.66 (0.07)
PFNA	1.94 (0.17)	0.60 (0.04)	3.10 (0.87)	1.09 (0.18)
PFDA	1.02 (0.57)	0.64 (0.07)	1.45 (1.40)	0.66 (0.16)
PFBS	0.25 (0.05)	0.26 (0.01)	0.15 (0.03)	0.73 (0.04)
PFHxS	1.18 (0.10)	0.52 (0.01)	1.09 (0.07)	1.24 (0.07)
PFOS	1.26 (0.02)	0.60 (0.01)	1.32 (0.11)	1.15 (0.04)
Gen X	0.17 (0.002)	0.46 (0.01)	0.16 (0.01)	1.06 (0.09)
		40°C		
PFOA	2.46 (0.16)	0.51 (0.01)	2.81 (0.06)	1.61 (0.04)

PFNA	1.93 (0.06)	0.60 (0.01)	4.12 (0.17)	0.65 (0.01)
PFDA	1.59 (1.03)	0.55 (0.01)	2.74 (0.54)	0.58 (0.08)
PFBS	0.19 (0.02)	0.33 (0.03)	0.41 (0.16)	0.73 (0.00)
PFHxS	1.17 (0.13)	0.52 (0.02)	1.29 (0.17)	0.96 (0.08)
PFOS	1.18 (0.16)	0.56 (0.003)	1.37 (0.23)	0.97 (0.00)
Gen X	0.12 (0.01)	0.53 (0.06)	0.17 (0.06)	1.46 (0.62)

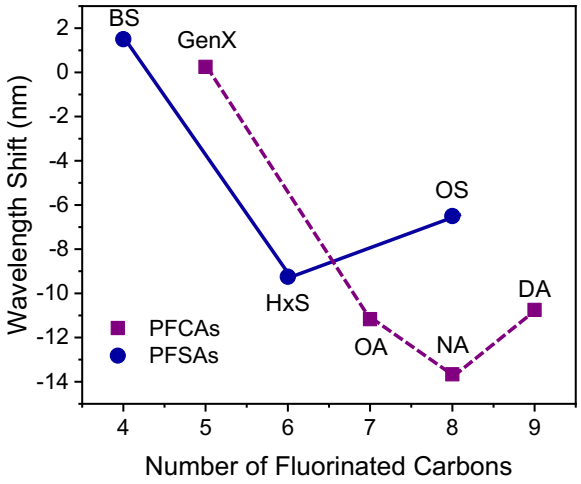

Figure S5. A representative plot of the shift in the wavelength of maximum fluorescence emission of BSA at 1.25 μM upon addition of PFAS at 68 μM at 25°C. A negative shift in maximum wavelength is indicative of a blue shift in the emission spectrum, which corresponds to the fluorophore experiencing a more hydrophobic environment.

REFERENCES

Allendorf, F., Berger, U., Goss, K.U., Ulrich, N., 2019. Partition coefficients of four perfluoroalkyl acid alternatives between bovine serum albumin (BSA) and water in comparison to ten classical perfluoroalkyl acids. Environ. Sci. Process. Impacts 21, 1852–1863.

https://doi.org/10.1039/c9em00290a

Berman, H.M., Battistuz, T., Bhat, T.N., Bluhm, W.F., Bourne, P.E., Burkhardt, K., Feng, Z., Gilliland, G.L., Iype, L., Jain, S., Fagan, P., Marvin, J., Padilla, D., Ravichandran, V., Schneider, B., Thanki, N., Weissig, H., Westbrook, J.D., Zardecki, C., 2002. The protein data bank. Acta Crystallogr. Sect. D Biol. Crystallogr. 58, 899–907. https://doi.org/10.1107/S0907444902003451

Majorek, K.A., Porebski, P.J., Dayal, A., Zimmerman, M.D., Jablonska, K., Stewart, A.J., Chruszcz, M., Minor, W., 2012. Structural and immunologic characterization of bovine, horse, and rabbit serum albumins. Mol. Immunol. https://doi.org/10.1016/j.molimm.2012.05.011

Sehnal, D., A.S. Rose, J. Kovca, S.K. Burley, S. Velankar (2018) Mol*: Towards a common library and tools for web molecular graphics MolVA/EuroVis Proceedings. https://doi.org/10.2312/molva.20181103